

Research Article

Fast Graph Partitioning Active Contours for Image Segmentation Using Histograms

Sumit K. Nath and Kannappan Palaniappan

Department of Computer Science, University of Missouri, Columbia, MO 65211, USA

Correspondence should be addressed to Kannappan Palaniappan, palaniappank@missouri.edu

Received 10 April 2009; Accepted 16 October 2009

Recommended by Nikos Nikolaidis

We present a method to improve the accuracy and speed, as well as significantly reduce the memory requirements, for the recently proposed Graph Partitioning Active Contours (GPACs) algorithm for image segmentation in the work of Sumengen and Manjunath (2006). Instead of computing an approximate but still expensive dissimilarity matrix of quadratic size, $(N_s^2 M_s^2)/(n_s m_s)$, for a 2D image of size $N_s \times M_s$ and regular image tiles of size $n_s \times m_s$, we use *fixed length histograms* and an intensity-based *symmetric-centrosymmetric extensor* matrix to *jointly* compute terms associated with the complete $N_s M_s \times N_s M_s$ dissimilarity matrix. This computationally efficient reformulation of GPAC using a very small memory footprint offers two distinct advantages over the original implementation. It speeds up convergence of the evolving active contour and seamlessly extends performance of GPAC to multidimensional images.

Copyright © 2009 S. K. Nath and K. Palaniappan. This is an open access article distributed under the Creative Commons Attribution License, which permits unrestricted use, distribution, and reproduction in any medium, provided the original work is properly cited.

1. Introduction

Recently, Sumengen and Manjunath have proposed a graph partitioning active contour (GPAC) algorithm for segmenting images motivated by graph cut approaches and parametric contour- or snake-based continuous curve evolution [1]. Using global minimization properties of graph partitioning methods, coupled with an efficient numerical implementation for solving curve evolution using level sets, GPAC produces impressive 2-class segmentation results for a variety of multichannel (e.g., RGB) images. Color segmentation using level sets has been previously reported in the literature (cf, Brox and Weickert [2], Bunyak et al. [3]). However, as noted by Sumengen and Manjunath in [1], these methods are based on the statistics of unknown regions and impose certain a priori assumptions about the image characteristics.

On the other hand, the underlying framework of GPAC is based on the minimum-cut formulation, a problem widely studied in the context of (color) image segmentation using graph cuts (cf, Boykov et al. [4]). GPAC reformulates the minimum-cut problem in a continuous domain and solves the problem using active contours, rather than graph-cuts [1].

The original description of the GPAC method follows an explicit parametric contour-based approach with Lagrangian dynamics. We start instead with an implicit level set description of the GPAC method following the notation of Chan and Vese [5] that provides better intuition and reveals the mathematical structure for the simplifying computations introduced later. Let $\phi(x)$ be a level set function used to segment a multichannel image in \mathbb{R}^2 , having dimensions $N_s \times M_s$. Using the Heaviside function, $H(\phi(x))$, we can write the normalized maximum-cut formulation of the GPAC energy functional combined with a length regularization term as

$$\begin{aligned} f_{\text{in}}(x) &= \int_{c \in \Omega} w(p, x) H(\phi(x)) dp, \\ f_{\text{out}}(x) &= \int_{c \in \Omega} w(p, x) (1 - H(\phi(x))) dp, \end{aligned} \quad (1)$$

where Ω is the complete image domain, integrals are multidimensional, $\lambda_1, \lambda_2, \mu$ are scalars associated with the functional, and $A_{\text{in}}, A_{\text{out}}$ are the areas of the evolving foreground and background regions, respectively. The last term in (1) is a regularization term that measures boundary length of the evolving level set and controls its smoothness.

The foreground and background homogeneity terms f_{in}, f_{out} are computed using the following weighted area integrals:

$$\begin{aligned} f_{in}(c) &= \int_{c \in \Omega} w(c, p) H(\phi(x)) dx, \\ f_{out}(c) &= \int_{c \in \Omega} w(c, p) (1 - H(\phi(x))) dx, \end{aligned} \quad (2)$$

where $w(p, x)$ is a symmetric dissimilarity measure between pixels located at indices c and p within a continuous domain Ω . In this paper we consider measures $w(c, p)$ that are a function of intensity only without measuring spatial differences between pixel locations as in the original GPAC implementation [1, 6].

Using Gâteaux derivatives, the Euler-Lagrange equation of (1) can be derived as

$$\frac{\partial \phi}{\partial t} = \delta(\phi) \left(\underbrace{\frac{\lambda_2}{A_{out}} f_{out} - \frac{\lambda_1}{A_{in}} f_{in}}_{\text{Data homogeneity term}} + \underbrace{\mu \operatorname{div} \left(\frac{\nabla \phi}{|\nabla \phi|} \right)}_{\text{Length regularization term}} \right). \quad (3)$$

The spatial index term (x) has been omitted for the sake of clarity. Similar to the original Chan-Vese algorithm, a regularized Heaviside and corresponding regularized Dirac-delta function, $\delta_\epsilon(\phi)$, should be used to improve the numerical stability of computing derivatives of a step-function. This will require appropriately adjusting the foreground mask in the proposed fast GPAC algorithm described below. The update equation shows that the level set iteration process will be slowed if homogeneity terms have to be recomputed at each iteration. Alternatively, precomputing dissimilarity measures between *all possible* pairs of pixels leads to tremendous storage requirements for even small sized images [1]. To resolve this difficulty, the image is partitioned into tiles of fixed dimensions (n_s, m_s) with $n_s \ll N_s, m_s \ll M_s$, and dissimilarity measures are precomputed with respect to centroids of these tiles, rather than each pixel [1, Section 4]. Various aspects of tile size selection have been discussed by the authors in [1, Section 4], including problems associated with selecting tiles across object boundaries, chances of the curve disappearing due to large tile sizes, and in general optimizing various scaling factors associated with the tile size. Recently, Bertelli et al. have used geodesic-based measures to optimize tile selection which requires the additional step of computing image edges and performing image-based region clustering [6]. Consequently, it would be preferable to forgo this tile-based (or super-pixel) solution of computing dissimilarity measures, and instead use exact dissimilarity measures (which is equivalent to setting $n_s = 1$ and $m_s = 1$) provided that computational efficiency can be addressed.

In Section 2, we propose the f-GPAC algorithm to compute dissimilarity measures using histograms, and a precomputed extensor matrix that is independent of pixel locations and instead depends entirely on the dynamic range pixel intensities. In Section 3, we provide comparative results between the f-GPAC and Sumengen and Manjunath's GPAC algorithm followed by conclusions in Section 4.

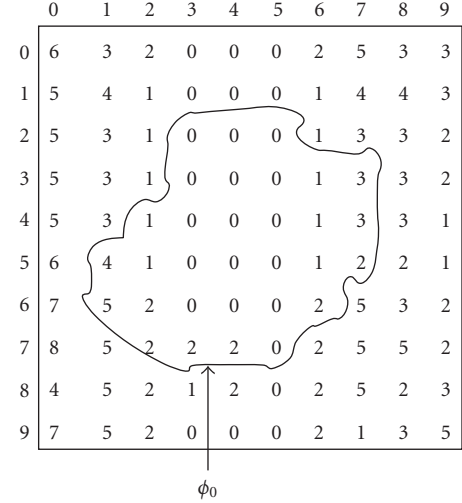


FIGURE 1: A 10×10 image with two distinct regions separated by a zero level set ϕ_0 . ($\mathcal{C}_1 \equiv \phi \geq 0$) and ($\mathcal{C}_2 \equiv \phi < 0$) represent the two regions (i.e., foreground and background) produced by the zero level set. The dynamic range of pixel intensities is between $\{I \in \mathbb{Z}^2 : I \in [0, 8]\}$.

2. Fast GPAC (f-GPAC) with Histograms

As highlighted in the previous section, an exact, rather than an approximate computation of the dissimilarity matrix W would lead to more consistent results during segmentation. For a better understanding in computing the dissimilarity matrix, let us use the example shown in Figure 1 that shows a 10×10 image with pixels having discrete integer intensity values $I \in [0, 8]$. We should mention that integer intensity values have been chosen for illustrative purposes only, and in the actual implementation intensities can be represented by any finite range of real numbers. Following [1], we arrange all pixels in a row-major order and compute elements of the 100×100 , location-dependent dissimilarity matrix (or graph edge-weights between pixels), W , as

$$W = \begin{array}{c|cccccc} I(i, j) & 6 & 5 & 5 & \cdots & 2 & 3 & 5 \\ \hline 6 & 0 & 1 & 1 & \cdots & 16 & 9 & 1 \\ 5 & 1 & 0 & 0 & \cdots & 9 & 4 & 0 \\ \vdots & \vdots \\ 3 & 9 & 4 & 4 & \cdots & 1 & 0 & 4 \\ 5 & 1 & 0 & 0 & \cdots & 9 & 4 & 0 \end{array} \quad (4)$$

It should be noted that in this paper we have constrained the dissimilarity measure to any suitable function of difference in intensity values (e.g., a squared Euclidean-distance measure). This is a more relaxed version of a general dissimilarity measure that incorporates differences in pixel position in addition to intensity differences between pixels in the original GPAC algorithm [1]. Clearly, precomputing dissimilarity measures for *all* pixels is redundant. For example, in the foreground region \mathcal{C}_1 , pixels with intensity $I(i, j) = 2$ occur six times. This redundancy makes computation, and storage

of \mathbf{W} a computationally expensive proposition. Hence, we propose a novel approach of exploiting this redundancy, thus leading to a highly efficient implementation of the GPAC algorithm.

Let us assume that an M channel image, in \mathbb{R}^2 , is being segmented into N classes (or regions) using K level sets. We do not constrain the relationship between K and N , but from the literature it is understood that $N = 2^K$ in a *dyadic multiphase* paradigm [7, 8], or $N = K + 1$ in other *nondyadic* paradigms (cf [9]). In the specific case of a single level set discussed in this paper, $N = 2$. Furthermore, we have a priori knowledge about the dynamic range of pixel intensities in all channels. Let I_{\min} and I_{\max} denote the minimum and maximum pixel intensities from all channels, so the dynamic range of pixel intensities $D = \lceil I_{\max} \rceil - \lceil I_{\min} \rceil + 1$.

First, we precompute a *symmetric centrosymmetric extensor matrix* \mathbf{P} as

$$P_{i,j} = (i - j)^2, \quad i \in [I_{\min}, I_{\max}], \quad j \in [I_{\min}, I_{\max}], \quad (5)$$

for the L_2 -squared norm or

$$P_{i,j} = |i - j|, \quad i \in [I_{\min}, I_{\max}], \quad j \in [I_{\min}, I_{\max}], \quad (6)$$

for the L_1 norm, to reflect *location independent* dissimilarity measures between pixel intensities. This intensity-domain distance matrix, whose dimensions depend on the intensity range and quantization bin-size, was inspired by the extensor matrix proposed by Palaniappan et al. [10, equation (1)], for solving problems related to image interpolation. In order to compute \mathbf{P} , we need to quantize the dynamic range of the image intensity, D . Although the intensity range can be quantized into any discrete set, a tradeoff needs to be made between using finer quantizations (i.e., more bins) and increasing the size of P , which would increase storage requirements. Note, however, that the storage requirement for the matrix \mathbf{P} does *not* increase quadratically with the number of quantization bins (i.e., D^2) since we only need to physically store the first row of the extensor matrix, and each subsequent row can be determined as needed through a sequence of shifts and copies. For the example shown in Figure 1, $I_{\min} = 0$, $I_{\max} = 8$, $D = 9$ and for an intensity quantization bin size of one, \mathbf{P} is a 9×9 matrix given by

$$\mathbf{P} = \begin{bmatrix} 0 & 1 & 4 & \cdots & 49 & 64 \\ 1 & 0 & 1 & \cdots & 36 & 49 \\ 4 & 1 & 0 & \cdots & 25 & 36 \\ \vdots & \vdots & \vdots & \cdots & \vdots & \vdots \\ 49 & 36 & 25 & \cdots & 0 & 1 \\ 64 & 49 & 36 & \cdots & 1 & 0 \end{bmatrix}. \quad (7)$$

Next, we exploit the redundancy in computing pixel intensity dissimilarities by constructing 1D histograms, $\mathbf{h}_{m,n}$, of each class from every channel in the image yielding MN histograms. The length of each histogram equals the dimension of the extensor matrix \mathbf{P} (i.e., D). Histograms have been previously used in level set segmentation, or to speed up

their implementation and is similar to a Chan and Vese style of modeling the image based on some sort of a priori characteristics [2], a fact highlighted at the beginning of this paper.

Thus, for the example shown in Figure 1, histograms for the two regions (i.e., $\mathbf{h}_{1,1}$ for \mathcal{C}_1 , and $\mathbf{h}_{1,2}$ for \mathcal{C}_2) are simply

$$\begin{array}{r} \mathbf{h}_{1,2}(\text{Background}) \\ \mathbf{h}_{1,1}(\text{Foreground}) \end{array} \begin{array}{cccccccc} 0 & 1 & 2 & 3 & 4 & 5 & 6 & 7 & 8 \\ 10 & 9 & 14 & 14 & 4 & 13 & 2 & 2 & 1 \\ 16 & 5 & 6 & 2 & 1 & 1 & 0 & 0 & 0 \end{array} \quad (8)$$

Using the permutation matrix and histograms we compute a vector of weights, $\mathbf{w}_{m,n}$, associated with pixels in each class, and for every channel using the following expression:

$$\mathbf{w}_{m,n} = \mathbf{P}\mathbf{h}_{m,n}, \quad n \in [1, N], \quad m \in [0, M - 1]. \quad (9)$$

The matrix-vector multiplication associated with (9) is used to update the active contour evolution and is performed at each level set iteration. This is not only a fixed cost operation but can be efficiently computed using Melmans algorithm in $(5/4)D^2 + O(D)$ floating point operations for a vector (i.e., histogram) of length D , instead of the $2D^2$ operations needed for an arbitrary matrix-vector multiplication [12].

By reducing the 2D M -channel image to a finite number of fixed length 1D histograms, we are able to remove the bottleneck of having to *explicitly* compute the dissimilarity matrix \mathbf{W} which as the authors noted in [1] makes segmentation an untenable operation, even for relatively small images unless suitable approximations are made. Furthermore, it is easy to observe that using a similar analogy, we can seamlessly extend our approach of computing histograms to segment images in higher dimensions \mathbb{R}^n , thus making f-GPAC a competitive alternative to other state-of-the-art segmentation methods.

Thus, computing the homogeneity (i.e., force) terms associated with each region in the original GPAC functional is equivalent to summing up intra-class homogeneity terms from each channel:

$$f_n[p] = \sum_{m=0}^{M-1} \mathbf{M}_n[p] \mathbf{w}_{m,n}[I[p, m]], \quad \text{and } n = 1, 2, \dots, N, \quad (10)$$

where $f_n[p]$ is a vector representing the discrete version of (2) for multichannel data with square brackets indicating array indexing, $I[p, m]$ is the intensity at the p th pixel location in the image from the m th channel, and the set of binary masks \mathbf{M}_n (obtained from a discrete, or crisp version of the Heaviside function) is used to select pixels from the n th region out of the N -classes, for each of M -channels.

To complement the previous discussion, steps of the algorithm for segmenting a multichannel 2D image (e.g., an RGB image) into two classes using a single level set are presented in Algorithm 1. The implementation of f-GPAC as described in Algorithm 1 pseudocode emphasizes clarity and in some steps can be further optimized for performance. The binary mask vector for class n , \mathbf{M}_n , is simplified to just \mathbf{M} for the foreground mask and $(1 - \mathbf{M})$ for the background mask

Input: \mathbf{I} , a 2D image with M -channels and 2-classes,
Input: \mathbf{M} , an initial 2D mask (binary)
 Scalars $\lambda_1, \lambda_2, \mu, \tau$, and, ϵ
 An appropriate stopping criterion
Output: ϕ_0^f , the final 2D mask (binary)

- (1) Compute I_{\min}, I_{\max} from all M -channels, and $D = \lceil I_{\max} \rceil - \lceil I_{\min} \rceil + 1$.
- (2) Compute the extensor matrix P and histograms for foreground and background from all M channels.
- (3) $A_{\text{in}}, A_{\text{out}}$, the foreground and background areas from \mathbf{M} .
- (4) Compute a signed Euclidean distance transform (EDT), ϕ_0^k , of \mathbf{M} using any suitable algorithm (cf, [11]).
- (5) **while** (!stopping criterion) **do**
- (6) Compute 1D weighting (of length D), using equation (9), for every channel $m \in [0, M - 1]$.
- (7) /*Update every pixel in the image*/
- (8) **for** $j = 0, 1, \dots, M_s N_s$ **do**
- (9) $f_1[j] = \sum_{m=0}^{M-1} \mathbf{M}[j] \mathbf{w}_{m,1}[I[j, m]], f_2[j] = \sum_{m=0}^{M-1} (1 - \mathbf{M}[j]) \mathbf{w}_{m,2}[I[j, m]]$
- (10) Update $\phi^k[j]$ to $\phi^{k+1}[j]$ using a semi-explicit discretization of (3) as in [5].
- (11) Update mask \mathbf{M} and histograms $\mathbf{h}_{m,n}$ for each channel and class, by noting sign changes in $\phi^{k+1} - \phi^k$.
- (12) Update mask \mathbf{M} .
- (13) Update A_{in} and A_{out} .
- (14) **end for**
- (15) **end while**
- (16) /*Binary mask from converged level set*/
- (17) $\phi_0^f \leftarrow \mathbf{M}$

ALGORITHM 1: Fast GPAC for 2-class image segmentation.

in the two-class ($N = 2$) case, and we use f_1 and f_2 for f_{in} and f_{out} , respectively (see (1)). For example, even though it is indicated that two histograms need to be maintained (and updated) for solving the two-class segmentation problem, it is easy to observe that, under certain conditions, this can be reduced to updating a single histogram. Using (10) and (9), and assuming the scaling terms $\lambda_1 = \lambda_2 = \lambda$, we can discretize and rewrite the data-homogeneity term of (3) as

$$\lambda \left(\frac{f_{\text{out}}}{A_{\text{out}}} - \frac{f_{\text{in}}}{A_{\text{in}}} \right) = \lambda \sum_{m=0}^{M-1} \mathbf{P} \left(\frac{\mathbf{h}_{m,2}}{A_{\text{out}}} - \frac{\mathbf{h}_{m,1}}{A_{\text{in}}} \right). \quad (11)$$

Let us simplify the term within braces. We know that the histogram of the complete image, $\mathbf{h} = \mathbf{h}_{1,1} + \mathbf{h}_{1,2}$, and the total area of the image $A_{\Omega} = A_{\text{in}} + A_{\text{out}}$. On replacing $\mathbf{h}_{1,2}$ and A_{out} in (11), the terms within the braces can be rewritten as

$$\begin{aligned} \lambda \sum_{m=0}^{M-1} \mathbf{P} \left(\frac{\mathbf{h}_{m,2}}{A_{\text{out}}} - \frac{\mathbf{h}_{m,1}}{A_{\text{in}}} \right) &= \lambda \sum_{m=0}^{M-1} \mathbf{P} \left(\frac{\mathbf{h} - \mathbf{h}_{m,1}}{A_{\Omega} - A_{\text{in}}} - \frac{\mathbf{h}_{m,1}}{A_{\text{in}}} \right) \\ &= \lambda \sum_{m=0}^{M-1} \mathbf{P} \left(\frac{A_{\text{in}} \mathbf{h} - A_{\Omega} \mathbf{h}_{m,1}}{((A_{\Omega} - A_{\text{in}}) A_{\text{in}})} \right) \\ &= \underbrace{\frac{\lambda_{\text{in}}}{A_{\Omega}} \sum_{m=0}^{M-1} \mathbf{P} \mathbf{h}}_{\text{Term 1}} - \underbrace{\frac{\lambda_{\text{in}}}{A_{\text{in}}} \sum_{m=0}^{M-1} \mathbf{P} \mathbf{h}_{m,1}}_{\text{Term 2}}, \end{aligned} \quad (12)$$

where

$$\lambda_{\text{in}} = \frac{\lambda A_{\Omega}}{A_{\Omega} - A_{\text{in}}}. \quad (13)$$

Clearly, Term 1 in (12) can be precomputed prior to beginning the iteration process. Hence the performance of f-GPAC can be made entirely dependent on updating a single histogram (Term 2—the histogram of the foreground region). The simplification described above is not valid if kernel-smoothing (e.g., Gaussian, cubic B-splines, etc.) is applied on the histograms prior to computing the homogeneity terms. However, kernel-smoothing on the image as a preprocessing step is not precluded by this simplification.

3. Experimental Results

We have implemented the proposed f-GPAC algorithm in MATLAB, utilizing calls to dynamic linked libraries written in C++ to optimize for speed. We have compared the performance of our algorithm with the original GPAC algorithm for which source code and test data are available online [13]. Unless otherwise mentioned, the same initial mask, as well as the following parameters, $\lambda_1 = N_s M_s$, $\lambda_2 = N_s M_s$, $\mu = 4.0 \times 10^4$, $\epsilon = 1.0$ were used in both algorithms. In addition, the following tile sizes have been used for the original GPAC algorithm: 4×4 , 8×8 , and 12×12 . In the original GPAC implementation, the level set iteration is deemed to have converged if the number of pixels changing signs in two consecutive iterations is less than a certain fixed number [13]. We have also used this stopping condition when implementing our algorithm. A semi-implicit discretization is used to solve the level set update equation (3). We omit details of this discretization and instead direct readers to [5, page 8, Section III].

Segmentation results of a few representative RGB images (with dimensions of 216×144) are described. For a

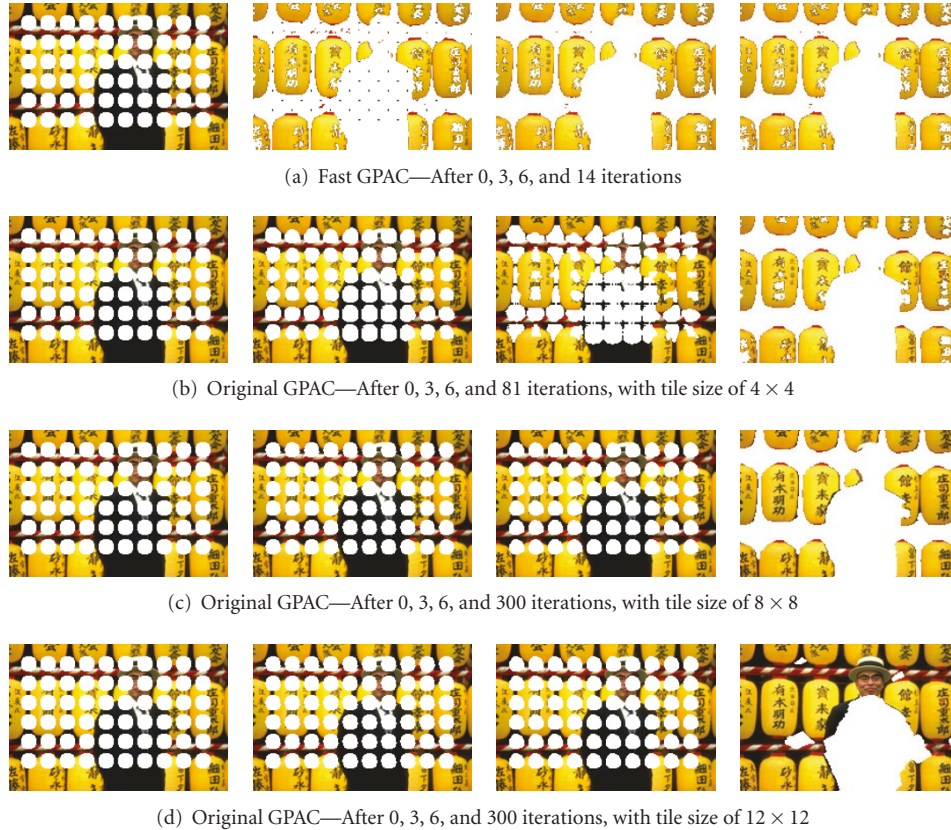


FIGURE 2: Comparative results of using our fast GPAC algorithm vis-à-vis the original GPAC algorithm in segmenting the “chinese_man” image. The RGB image was transformed into the YCbCr space prior to segmentation. It can be noted that decreasing the tile size improves the convergence rate of the level set segmentation (indicated by the white mask). On the other hand, convergence is reached after 14 iterations when using the f-GPAC algorithm. The stopping criterion is satisfied if less than 30 pixels change signs between two successive iterations, or a count of 300 iterations is reached.

perceptual uniform color-space and faster convergence, RGB images were transformed to the YCbCr space and suitably scaled, prior to segmentation. We shift the dynamic range of the image components using the experimentally determined transformation, Y-10, Cb-20, and, Cr-20. We have observed that recentering the color component histograms improves the final image segmentation results. An L_2 -squared intensity-based extensor distance matrix (as shown in (5)) of size 256×256 (and storing only the first row, as described in Section 2) was used in all the experiments.

As shown in Figure 2, approximate versions of the original GPAC algorithm lead to a longer convergence time (4×4 tile sizes), or incorrect segmentation (12×12 tile sizes). In contrast, our f-GPAC algorithm correctly extracts out the man and similar regions (e.g., Chinese characters) from the image. Using the same parameters, we notice a nearly 7-fold decrease in convergence time when compared to the original GPAC algorithm using the smallest possible tile size dimension. Unfortunately, using the original GPAC algorithm, further reduction in tile size was not possible due to the huge amount of memory needed for storing the dissimilarity matrix. A similar set of observations can be drawn when segmenting other images having similar dimensions (e.g., “horses” and “starfish” in Figure 3).

The f-GPAC algorithm produces nearly the same (or better) results as the original GPAC algorithm, using the smallest computationally feasible tile size for the latter, and f-GPAC also demonstrates faster convergence. Moreover, as observed in [1] increasing tile sizes can lead to unreliable results as seen in Figure 3, where the tile size is increased to 12×12 . We wish to emphasize that changing the scaling parameters associated with the level set functional may lead to improved results using the original GPAC method. In our f-GPAC implementation we have avoided this approach and used the same set of parameters for segmenting all images described in the experiments. However, we do acknowledge that even in our algorithm, some parameters may need to be changed (e.g., μ that controls smoothness of the curve) when segmenting different classes of images.

In the context of biological image analysis, accurate image partitioning is an important step when segmenting and tracking multiple closely touching objects, such as cells (cf [14–16]), when biological objects such as plant or animal tissues need to be detected in highly cluttered and noisy surroundings ([17–19]), or when complex biopsy tissues are segmented into their constitutive elements [8, 20]. We have compared the performance of f-GPAC, as well as the original GPAC algorithm in clustering nuclei from

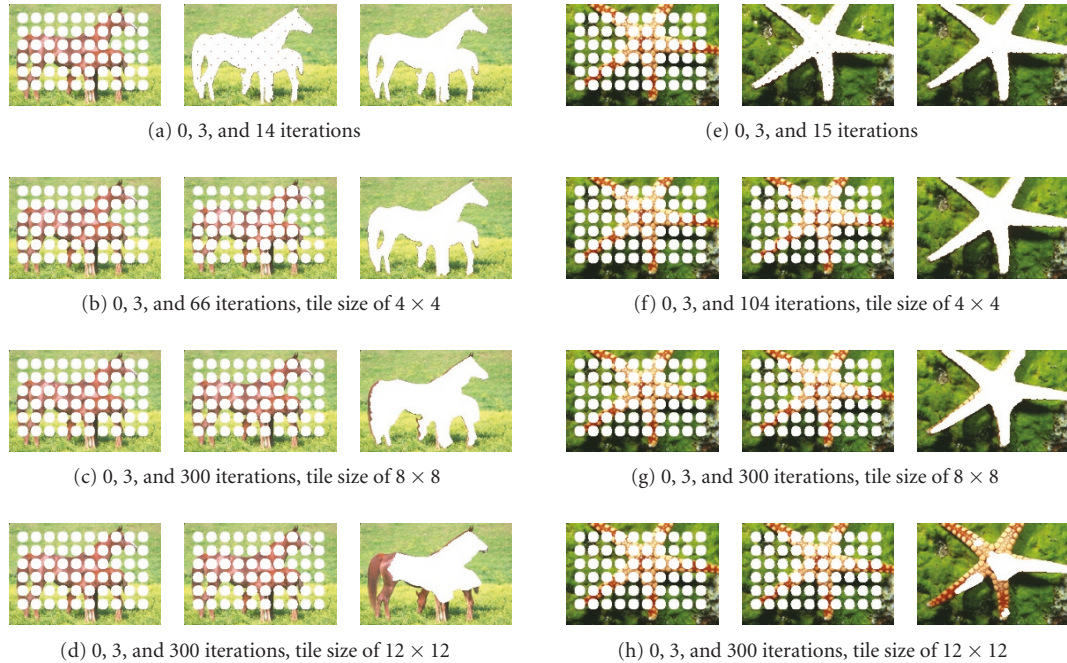


FIGURE 3: Comparative results at various iteration steps when using our fast GPAC algorithm ((a) and (e)) vis-à-vis the original GPAC algorithm ((b)–(d), and (f)–(h)) in segmenting “horses” and “starfish” images. The parameters, used in segmenting the “chinese_man” image (Figure 2), were also used in segmenting these images.

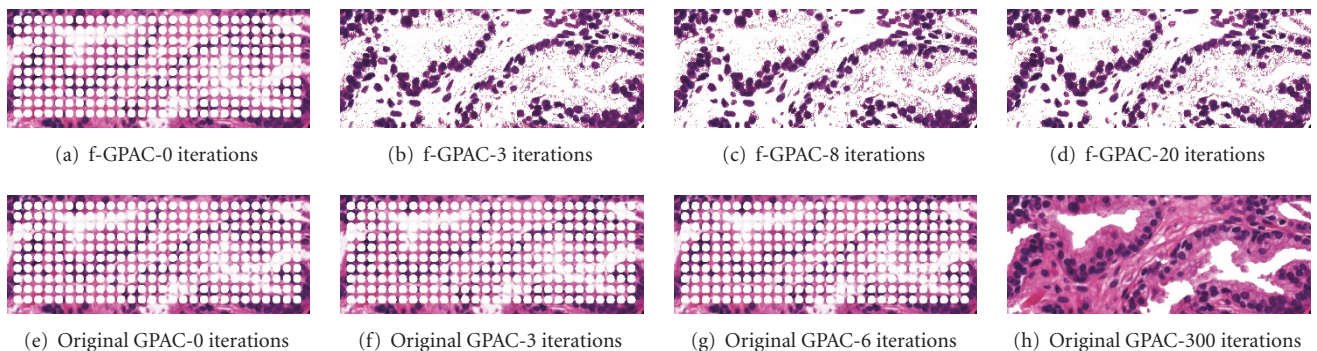


FIGURE 4: Comparative results of using the f-GPAC algorithm vis-à-vis the original GPAC algorithm in segmenting “benign_cells” with dimensions 557×227 . The minimum tile size that could be used in the original GPAC algorithm was 12×12 . The stopping condition was set at 60 pixels, or a maximum iteration count of 300. Other parameters (like λ_1 , λ_2 , etc.) were the same as that used in generating results shown in Figure 3. Evidently, the f-GPAC algorithm correctly segments the background (i.e., noncellular regions), while the original GPAC is only able to segment stromal (white) regions in the image.

hematoxylin and eosin (H&E) stained images of biopsy tissue cores containing various grades of prostate cancer including, “benign_cells” (Figure 4), “grade3_cells” (Figure 5), and “grade4_cells” (Figure 6), respectively. With small tile sizes the original GPAC algorithm cannot be used for segmenting large images (e.g., “grade4_cells”), while using a larger tile size (e.g., 14×14) leads to the eventual disappearance of the evolving curve! However, using the proposed f-GPAC algorithm, a clear demarcation between cellular clusters and the background is achieved in all cases, within 60 iterations. The stopping criterion was changed from 30 to 60 pixels, and the upper bound on the number of iterations set to 300 for this dataset.

The difficulty in using the original GPAC and the advantage of using the proposed f-GPAC for segmenting large images, such as the “grade4_cells” image, merit further discussion. A minimum tile size of 14×14 is the smallest that could be used to compute the dissimilarity matrix. Due to large memory requirements of storing the dissimilarity matrix, we could not use a smaller tile size. However, as seen from Figure 6(b), the evolving curve eventually disappears when using this large of a tile size. This confirms the observation made by the authors in [1, Section IV], that when large tile sizes are used in the original GPAC implementation, the curve may shrink and disappear instead of converging to an object boundary. When the

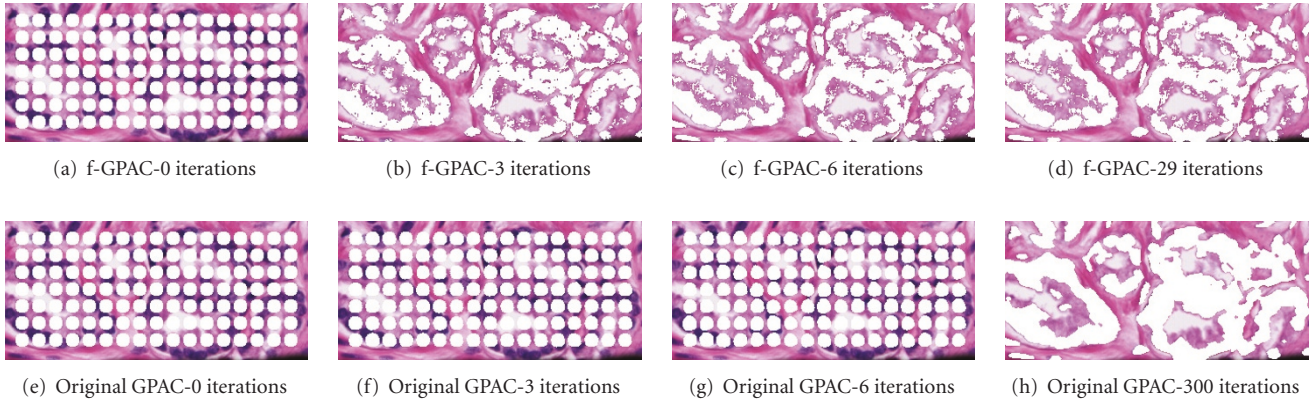


FIGURE 5: Comparative results of using the f-GPAC algorithm vis-à-vis the original GPAC algorithm in segmenting “grade3_cells” with dimensions 340×156 . The minimum tile size that could be used in the original GPAC algorithm was 5×5 . The stopping condition was set at 60 pixels, or a maximum iteration count of 300. Other parameters (like λ_1 , λ_2 , etc.) were the same as those used in generating results shown in Figure 3. Evidently, both the f-GPAC, as well as the original GPAC algorithm correctly segment the foreground (i.e., cellular regions). However, the large value of μ results in smoothed blobs when using the original GPAC. Fine details of cell boundaries are preserved when using the f-GPAC algorithm.

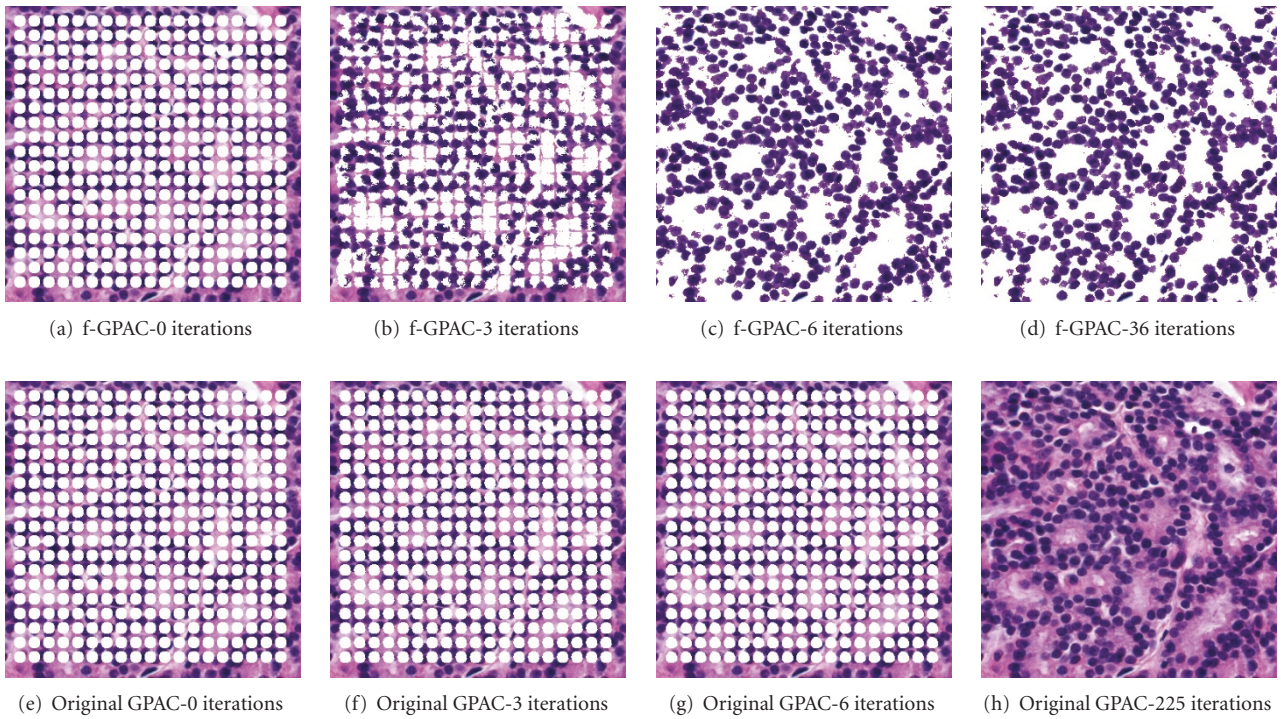


FIGURE 6: Comparative results of using the f-GPAC algorithm vis-à-vis the original GPAC algorithm in segmenting “grade4_cells” with dimensions 388×389 . The minimum tile size that could be used in the original GPAC algorithm was 14×14 , was the same as that used in generating results shown in Figure 5. The selected tile size for the GPAC algorithm leads to the disappearance of the evolving curve. Please refer to the text for more details.

tile size is sufficiently reduced then a correct segmentation is achieved using the original GPAC algorithm (Figure 4). However, there is excessive smoothing of boundaries in the segmented region due to a combination of using image tiling and without tuning μ .

4. Conclusions

A novel approach to improve the performance of the GPAC algorithm, proposed by Sumengen and Manjunath, has been presented in this paper. We, jointly, compute terms associated

with various elements of the complete dissimilarity matrix by fixed length histograms and an intensity-based circulant symmetric-centrosymmetric extensor distance matrix, thus obviating the need to use spatial approximations to the dissimilarity matrix. This dramatically reduces the memory requirement for GPAC as image size increases while still computing exact weights, which in turn leads to faster convergence, and accurate segmentation when compared with the original GPAC algorithm. Opportunities for further improving the performance of f-GPAC include using a narrow-band implementation by maintaining a list of narrow-band pixels around the zero level set and updating only those pixels [9]. This approach is useful when a good initial guess is provided to the f-GPAC algorithm. Parallelization using additive operator splitting (AOS) can also be employed when updating the Euler-Lagrange equation for f-GPAC (cf [21, 22]) to further speed-up performance. The proposed f-GPAC algorithm improves the applicability of GPAC for a wide range of image segmentation tasks and offers scalability to explore automatic segmentation of large multidimensional datasets.

Acknowledgments

The authors would like to thank the U.S. National Institute of Health and the U.S. Department of Defence for financial support that made this research possible. In addition, the authors would like to thank Luca Bertelli and B. S. Manjunath at the University of California, Santa Barbara for fruitful discussions related to various implementation details of the GPAC algorithm, and Michael Feldman at the University of Pennsylvania, Philadelphia for providing prostate cancer images used in testing the f-GPAC algorithm. This work was initiated at the University of Missouri-Columbia under a U.S. National Institute of Health NIBIB award R33 EB00573 and completed at Rensselaer Polytechnic Institute, Troy with kind support from Dr. Badrinath Roysam under a U.S. DOD Cancer Research Program IDEA Grant BC061142.

References

- [1] B. Sumengen and B. Manjunath, "Graph partitioning active contours (GPAC) for image segmentation," *IEEE Transactions on Pattern Analysis and Machine Intelligence*, vol. 28, no. 4, pp. 509–521, 2006.
- [2] T. Brox and J. Weickert, "Level set based image segmentation with multiple regions," in *Proceedings of the 26th Pattern Recognition Symposium (DAGM '04)*, vol. 3175 of *Lecture Notes in Computer Science*, pp. 415–423, Tubingen, Germany, August 2004.
- [3] F. Bunyak, K. Palaniappan, S. Nath, and G. Seetharaman, "Flux tensor constrained geodesic active contours with sensor fusion for persistent object tracking," *Journal of Multimedia*, vol. 2, no. 4, pp. 20–33, 2007.
- [4] Y. Boykov, O. Veksler, and R. Zabih, "Fast approximate energy minimization via graph cuts," *IEEE Transactions on Pattern Analysis and Machine Intelligence*, vol. 23, no. 11, pp. 1222–1239, 2001.
- [5] T. Chan and L. Vese, "Active contours without edges," *Tech. Rep. CAM98-53*, Department of Mathematics, UCLA, Los Angeles, Calif, USA, December 1998, <ftp://ftp.math.ucla.edu/pub/camreport/cam98-53.ps.gz>.
- [6] L. Bertelli, B. Sumengen, B. S. Manjunath, and F. Gibou, "A variational framework for multi-region pairwise similarity-based image segmentation," *IEEE Transactions on Pattern Analysis and Machine Intelligence*, vol. 30, no. 8, pp. 1400–1414, 2008.
- [7] L. A. Vese and T. F. Chan, "A multiphase level set framework for image segmentation using the Mumford and Shah model," *International Journal of Computer Vision*, vol. 50, no. 3, pp. 271–293, 2002.
- [8] A. Hafiane, F. Bunyak, and K. Palaniappan, "Clustering initiated multiphase active contours and robust separation of nuclei groups for tissue segmentation," in *Proceedings of the 19th International Conference on Pattern Recognition (ICPR '08)*, pp. 1–4, Tampa, Fla, USA, December 2008.
- [9] S. Nath, K. Palaniappan, and F. Bunyak, "Cell segmentation using coupled level sets and graph-vertex coloring," in *Proceedings of the 9th International Conference on Medical Image Computing and Computer-Assisted Intervention (MICCAI '06)*, vol. 4190 of *Lecture Notes in Computer Science*, pp. 101–108, Springer, Copenhagen, Denmark, October 2006.
- [10] K. Palaniappan, J. Uhlmann, and D. Li, "Extensor-based image interpolation," in *Proceedings of IEEE International Conference on Image Processing (ICIP '03)*, vol. 2, pp. 945–948, Barcelona, Spain, September 2003.
- [11] P. Felzenswalb and D. Huttenlocher, "Distance transforms of sampled functions," *Tech. Rep. TR2004-1963*, Department of Computer Science, Cornell University, Ithaca, NY, USA, September 2004, <http://people.cs.uchicago.edu/~pff/papers/dt.pdf>.
- [12] A. Melman, "Symmetric centrosymmetric matrix-vector multiplication," *Linear Algebra and Its Applications*, vol. 320, no. 1–3, pp. 193–198, 2000.
- [13] http://vision.ece.ucsb.edu/~lbartelli/soft_GPAC.html.
- [14] A. Mosig, S. Jäeger, W. Chaofeng, et al., "Tracking cells in live cell imaging videos using topological alignments," *Algorithms for Molecular Biology*, vol. 4, article 10, pp. 1–9, 2009.
- [15] S. K. Nath, F. Bunyak, and K. Palaniappan, "Robust tracking of migrating cells using four-color level set segmentation," in *Proceedings of the 8th International Conference on Advanced Concepts for Intelligent Vision Systems (ACIVS '06)*, vol. 4179 of *Lecture Notes in Computer Science*, pp. 920–932, Antwerp, Belgium, September 2006.
- [16] F. Bunyak, K. Palaniappan, S. K. Nath, T. I. Baskin, and D. Gang, "Quantitative cell motility for in vitro wound healing using level set-based active contour tracking," in *Proceedings of the 3rd IEEE International Symposium on Biomedical Imaging (ISBI '06)*, pp. 1040–1043, Arlington, Va, USA, April 2006.
- [17] G. Dong, T. I. Baskin, and K. Palaniappan, "Motion flow estimation from image sequences with applications to biological growth and motility," in *Proceedings of the IEEE International Conference on Image Processing (ICIP '06)*, pp. 1245–1248, Atlanta, Ga, USA, October 2006.
- [18] C. M. van der Weele, H. S. Jiang, K. K. Palaniappan, V. B. Ivanov, K. Palaniappan, and T. I. Baskin, "A new algorithm for computational image analysis of deformable motion at high spatial and temporal resolution applied to root growth. Roughly uniform elongation in the meristem and also, after an abrupt acceleration, in the elongation zone," *Plant Physiology*, vol. 132, no. 3, pp. 1138–1148, 2003.
- [19] K. Palaniappan, H. Jiang, and T. I. Baskin, "Non-rigid motion estimation using the robust tensor method," in *Proceedings of the Conference on Computer Vision and Pattern Recognition*

Workshop (CVPRW '04), pp. 25–33, IEEE Computer Society, Washington, DC, USA, June-July 2004.

- [20] A. Hafiane, F. Bunyak, and K. Palaniappan, “Fuzzy clustering and active contours for histopathology image segmentation and nuclei detection,” in *Proceedings of the 10th International Conference on Advanced Concepts for Intelligent Vision Systems (ACIVS '08)*, vol. 5259 of *Lecture Notes in Computer Science*, pp. 903–914, Springer, Juan-les-Pins, France, October 2008.
- [21] J. Weickert, B. M. Ter Haar Romeny, and M. A. Viergever, “Efficient and reliable schemes for nonlinear diffusion filtering,” *IEEE Transactions on Image Processing*, vol. 7, no. 3, pp. 398–410, 1998.
- [22] K. Palaniappan, I. Ersoy, and S. K. Nath, “Moving object segmentation using the flux tensor for biological video microscopy,” in *Proceedings of the 8th Pacific-Rim Conference on Multimedia (PCM '07)*, vol. 4810 of *Lecture Notes in Computer Science*, pp. 483–493, Springer, Hong Kong, December 2007.